

Thévenin Equivalent Parameters Identification Based on Statistical Characteristics of System Ambient Data

Boying Zhou, *Student Member, IEEE*, Chen Shen, *Senior Member, IEEE*, and Kexuan Tang, *Student Member, IEEE*

Abstract—This paper proposes a novel method for identifying Thévenin equivalent parameters (TEP) in power system, based on the statistical characteristics of the system’s stochastic response. The method leverages stochastic fluctuation data under steady-state grid conditions and applies sliding window techniques to compute sensitivity parameters between voltage magnitude, current magnitude and power. This enables high-accuracy and robust TEP identification. In contrast to traditional methods, the proposed approach does not rely on large disturbances or probing signals but instead utilizes the natural fluctuation behavior of the system. Additionally, the method supports distributed implementation using local measurements of voltage magnitude, current magnitude, and power, offering significant practical value for engineering applications. The theoretical analysis demonstrates the method’s robustness in the presence of low signal-to-noise ratio (SNR), asynchronous measurements, and data collinearity issues. Simulation results further confirm the effectiveness of the proposed method in diverse practical scenarios, demonstrating its ability to consistently provide accurate and reliable identification of TEP using system ambient data.

Index Terms—Thévenin equivalent parameters, sensitivity analysis, ambient data, statistical characteristics, sliding window techniques, low SNR, asynchronous measurements, data collinearity.

I. INTRODUCTION

A. Motivation

THÉVENIN equivalent (TE) serves as a core tool for assessing power system stability and safety. By simplifying complex networks into an equivalent voltage source and impedance, TE provides precise and efficient tools for steady-state analyses (e.g., power flow and voltage stability) and transient fault diagnosis (e.g., short-circuit current). With the widespread adoption of PMU technology, interest in online identification and monitoring of Thévenin equivalent parameters (TEP) using PMU data has increased [1].

Traditional data-driven methods for TEP identification rely on system disturbances or probing signal injection, requiring significant disturbances to achieve clearer response characteristics, which improves the signal-to-noise ratio (SNR) and enhances the accuracy of TEP identification.

This work was supported by the The National Key R&D Program of China “Response-driven intelligent enhanced analysis and control for bulk power system stability” under Grant 2021YFB2400800. Paper no. TPWRS-00750-2024. (*Corresponding author: Chen Shen.*)

The authors are with the Department of Electrical Engineering, Tsinghua University, Beijing 100084, China (e-mail: zby21@mails.tsinghua.edu.cn; shenchen@mail.tsinghua.edu.cn; 14z32@163.com).

However, under steady-state conditions, large disturbances are rare, and power system typically maintains a stable topology and operating mode. In this context, electrical measurements are primarily influenced by stochastic fluctuations, such as load variations and renewable energy output changes [2]. These stochastic fluctuations, superimposed on steady-state operation, provide insufficient information for traditional methods, reducing the reliability and robustness of parameter identification.

Furthermore, to ensure accurate identification results, traditional data-driven TEP identification methods typically rely on high-precision PMU synchronized measurements. This reliance significantly reduces the method’s applicability and robustness when measurement noise or synchronization issues arise [3].

Considering the limitations of traditional methods under steady-state conditions of the power system, this paper aims at proposing a novel method for TEP identification based on the statistical characteristics of the system’s stochastic response. By exploiting the stochastic fluctuations in ambient data and analyzing their statistical variations, this approach enables robust and accurate identification of TEP under steady-state conditions.

B. Literature Review

The method based on a limited number of measurement samples is one of the simplest and earliest approaches for TEP identification. It uses local measurement data (typically from two or more adjacent time points) to identify model parameters by analyzing changes in port measurements between time instants [1]. Due to its simplicity and ease of implementation, it is widely used in practical power systems. However, it assumes that system-side model parameters remain constant during identification [4], which hinders the accurate capture of dynamic system characteristics. Additionally, the accuracy of this method is highly dependent on the selection of measurement points, making it vulnerable to nonlinearity and measurement noise, leading to significant errors in parameter estimation [5].

PMU data can deviate from actual values due to external disturbances or system faults [6]. To address the limitations of traditional methods, several improved algorithms based on least squares (LS) and its variants have been proposed, such as classical LS [7], [8], robust LS [9], [10], recursive LS with

variable forgetting factors [11], and constrained LS [12]. These methods typically require large data windows to minimize estimation errors caused by voltage and current phasor errors and transients, which can delay the estimation process. To mitigate this, Ref. [13] employs the dynamic updating mechanism of the Kalman filter to reduce errors and noise. Ref. [14] improves accuracy by using multiple measurements within a time window, applying techniques like error elimination or weighting. Ref. [15] uses an extended Kalman filter with equivalent constraints and statistical projection to enhance robustness, while Ref. [16] introduces a multivariate Huber loss function to address estimation issues under non-Gaussian noise.

In recent years, sensitivity analysis-based algorithms have emerged as a prominent approach for TEP identification. These methods estimate parameters based on the system's sensitivity to input disturbances, making them well-suited for scenarios with frequent system dynamic changes [17]. For instance, Ref. [18] derives the relationship between the linear Thévenin index and sensitivity, introducing the Sensitivity-Based Thévenin Index (STI) for monitoring long-term voltage stability. Ref. [19] uses Tellegen's theorem to derive equivalent impedance expressions, further refining the STI. Additionally, Ref. [20] extends the STI to evaluate voltage stability under N-1 transmission line faults.

However, the inherent nonlinearities, collinearity, and periodic characteristics of power systems often result in insufficient data for accurate sensitivity parameter identification [21]. Online sensitivity information may also lead to inaccurate estimations. To mitigate these issues, Ref. [22] applies Total Least Squares (TLS) to handle data collinearity. Ref. [23] employs ridge regression to estimate sensitivity coefficients and introduces directional forgetting to address instability during low-excitation periods. Ref. [24] combines local weighted ridge regression with Tikhonov-Phillips regularization to stabilize sensitivity identification under collinearity. Ref. [25] uses adaptive weighted sparsity-promoting regularization with the Huber loss function to reduce collinearity and mitigate non-Gaussian noise effects. Ref. [26] proposes a sensitivity estimation method considering mutual dependency in medium-voltage distribution networks.

Although significant progress has been made in addressing noise, collinearity, and data anomalies in sensitivity parameter and TEP identification methods, their effectiveness under steady-state conditions remains limited. In such conditions, electrical measurements from both the system and the load side are primarily affected by stochastic fluctuations, with system measurement noise having a substantial impact on results. Traditional methods fail to fully exploit the statistical characteristics inherent in these fluctuations, leading to significant identification errors in low signal-to-noise ratio (SNR) condition or when disturbances are minimal.

Thus, achieving efficient and accurate TEP identification using only stochastic fluctuation data remains a critical challenge that requires further attention.

C. Contribution

In this paper, we propose a new method for identifying TEP based on the statistical characteristics of the system's stochastic response. The method utilizes ambient data under steady-state conditions, calculating the statistical properties of stochastic fluctuations through a sliding window technique, and accurately identifies the sensitivity parameters between voltage magnitude and power, as well as current magnitude and power, thereby achieving high-precision and robust TEP identification under steady-state conditions. In summary, the contributions of this paper are as follows:

- 1) A new method for TEP identification based on the statistical characteristics of system's stochastic response is proposed. This method calculates the statistical properties of stochastic fluctuations within a sliding window, accurately estimating sensitivity parameters between voltage magnitude, current magnitude, and power. It achieves high-precision TEP identification using only ambient data, unlike traditional methods that rely on large disturbances or probe signals.
- 2) The method's robustness under low SNR is demonstrated. The SNR of the statistical characteristics from measurement data is higher than the original data due to the difference in correlation between stochastic fluctuations and measurement noise. This results in improved TEP identification accuracy in low SNR conditions, overcoming the traditional reliance on high SNR.
- 3) The method is also robust under asynchronous measurements. The relative error of statistical characteristics data from the sliding window is lower than that of the original data. This approach improves TEP identification accuracy in asynchronous measurement situations, addressing the traditional dependence on synchronized measurements.
- 4) The method performs well even with data collinearity. It does not significantly increase the correlation or condition number of the data. When low SNR, asynchronous measurements, and data collinearity are present, the optimal method can be selected using decentralized condition number inequalities.

The rest of this paper is organized as follows. Section II presents the method for TEP identification based on magnitude sensitivity. Section III introduces the method for precise magnitude sensitivity identification based on stochastic response statistical characteristics and proves that the proposed method offers advantages in identification accuracy under low SNR, asynchronous measurements, and data collinearity. Section IV validates the effectiveness of the proposed identification method through simulation examples. Finally, conclusions are provided in Section VII.

II. TEP IDENTIFICATION BASED ON MAGNITUDE SENSITIVITY

A. Thévenin Equivalent Model

The schematic diagram for Thevenin equivalent (TE) in a power system is shown in Figure 1. This method divides the power system at the equivalent port (load node or flow

interface) into two parts: the "equivalent side" and the "load side." The "equivalent side" is represented as a TE voltage source in series with a TE impedance, as shown in Fig. 1.

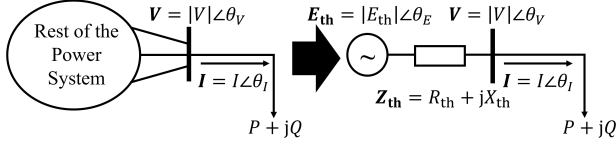


Fig. 1. Schematic diagram of Thévenin equivalent in a power system.

In Fig. 1, $|E_{th}|$ and θ_E represent the magnitude and phase angle of the TE voltage source E_{th} . Z_{th} represents the TE impedance, with R_{th} as the TE resistance and X_{th} as the TE reactance. $|V|$ and θ_V represent the magnitude and phase angle of the port voltage V . $|I|$ and θ_I represent the magnitude and phase angle of the current I flowing from the equivalent side through the port to the load side. P and Q represent the real and reactive power flowing from the equivalent side through the port to the load side.

The TEP used for voltage stability analysis are the equivalent voltage magnitude $|E_{th}|$, equivalent resistance R_{th} , and equivalent reactance X_{th} .

According to Kirchhoff's Voltage Law and the definition of power, the parameters of the equivalent port satisfy the relationships as

$$\begin{cases} E_{th} = I \cdot Z_{th} + V \\ P + jQ = V \cdot I^* \end{cases} \quad (1)$$

By converting the phasor relationship in Eq.(1) into a magnitude relationship equation, we derive the relationships for port voltage magnitude $|V|$, port current magnitude $|I|$, active power P , and reactive power Q as

$$\begin{cases} |V|^4 + (R_{th}^2 + X_{th}^2)(P^2 + Q^2) \\ \quad + (2R_{th}P + 2X_{th}Q - |E_{th}|^2)|V|^2 = 0 \\ (R_{th}^2 + X_{th}^2)|I|^4 + (P^2 + Q^2) \\ \quad + (2R_{th}P + 2X_{th}Q - |E_{th}|^2)|I|^2 = 0 \end{cases} \quad (2)$$

By solving the magnitude relationship equation in Eq.(2), the theoretical solution for the port voltage and current magnitude at the stable operating point can be obtained, as shown as

$$\begin{cases} |V| = \sqrt{\frac{|E_{th}|^2 - 2(R_{th}P + X_{th}Q) + \sqrt{\Delta}}{2}} \\ |I| = \sqrt{\frac{|E_{th}|^2 - 2(P R_{th} + Q X_{th}) - \sqrt{\Delta}}{2(R_{th}^2 + X_{th}^2)}} \end{cases} \quad (3)$$

where discriminant $\Delta = |E_{th}|^4 - 4(R_{th}P + X_{th}Q)|E_{th}|^2 - 4(X_{th}P - R_{th}Q)^2$.

B. Magnitude Sensitivity Based Identification of TEP

Considering that sensors at the boundaries of distribution and transmission networks typically cannot measure voltage phase angles [27], this paper employs magnitude sensitivity for TEP identification, aiming to broaden the applicability of the

method. The voltage magnitude-power sensitivity and current magnitude-power sensitivity quantify the responsiveness of the port voltage and current magnitude to power changes, respectively. Sensitivity analysis assumes that, within a small range, the changes in voltage and current magnitude exhibit a linear response to variations in active and reactive power, as shown as

$$\begin{bmatrix} \Delta |V| \\ \Delta |I| \end{bmatrix} \approx \begin{bmatrix} \frac{\partial |V|}{\partial P} & \frac{\partial |V|}{\partial Q} \\ \frac{\partial |I|}{\partial P} & \frac{\partial |I|}{\partial Q} \end{bmatrix} \begin{bmatrix} \Delta P \\ \Delta Q \end{bmatrix} = \begin{bmatrix} \beta_{|V|P} & \beta_{|V|Q} \\ \beta_{|I|P} & \beta_{|I|Q} \end{bmatrix} \begin{bmatrix} \Delta P \\ \Delta Q \end{bmatrix} \quad (4)$$

where $\Delta|V|, \Delta|I|, \Delta P$, and ΔQ represent the variations of voltage magnitude, current magnitude, active power, and reactive power. $\beta_{|V|P}$ and $\beta_{|V|Q}$ denote the sensitivity parameters of voltage magnitude with respect to changes in active and reactive power, while $\beta_{|I|P}$ and $\beta_{|I|Q}$ represent the sensitivity parameters of current magnitude with respect to changes in active and reactive power. These four sensitivity parameters are collectively referred to as the magnitude sensitivity parameters.

Using the theoretical values from Eq.(3), the partial derivatives of voltage and current magnitude with respect to active and reactive power are calculated. The resulting theoretical values of the port magnitude sensitivity parameters are presented as

$$\begin{cases} \beta_{|V|P} = -\frac{(R_{th}^2 + X_{th}^2)\tilde{P}_k + R_{th}|\tilde{V}_k|^2}{|\tilde{V}_k|\sqrt{\tilde{\Delta}}} \\ \beta_{|V|Q} = -\frac{(R_{th}^2 + X_{th}^2)\tilde{Q}_k + X_{th}|\tilde{V}_k|^2}{|\tilde{V}_k|\sqrt{\tilde{\Delta}}} \\ \beta_{|I|P} = \frac{\tilde{P}_k + R_{th}|\tilde{I}_k|^2}{|\tilde{I}_k|\sqrt{\tilde{\Delta}}} \\ \beta_{|I|Q} = \frac{\tilde{Q}_k + X_{th}|\tilde{I}_k|^2}{|\tilde{I}_k|\sqrt{\tilde{\Delta}}} \end{cases} \quad (5)$$

where discriminant $\tilde{\Delta} = |E_{th}|^4 - 4(R_{th}\tilde{P}_k + X_{th}\tilde{Q}_k)|E_{th}|^2 - 4(X_{th}\tilde{P}_k - R_{th}\tilde{Q}_k)^2$. $|\tilde{V}_k|$, $|\tilde{I}_k|$, \tilde{P}_k , and \tilde{Q}_k represent the real-time measurements of electrical quantities. Eq.(5) reflects the nonlinear relationship between the magnitude sensitivity parameters and TEP.

When the sensitivity parameters are accurately identified, the true values of the Thévenin equivalent parameters can be determined as the common solution of the theoretical equations Eq.(3) and the sensitivity parameters equations Eq.(5). To improve the accuracy of parameter identification, Eq.(3) and Eq.(5) can be combined into a system of six-order overdetermined nonlinear equations, as shown in Eq.(6). The full set of equations can be found in App.A.

$$\begin{cases} \{\beta_{|V|P}, \beta_{|V|Q}, \beta_{|I|P}, \beta_{|I|Q}\} \\ = \mathbf{f} \left(|E_{th}|, R_{th}, X_{th}, \tilde{P}_k, \tilde{Q}_k, |\tilde{I}_k|, |\tilde{V}_k| \right) \\ \left\{ |\tilde{V}_k|, |\tilde{I}_k| \right\} = \mathbf{f} \left(|E_{th}|, R_{th}, X_{th}, \tilde{P}_k, \tilde{Q}_k \right) \end{cases} \quad (6)$$

Based on the identification results of the magnitude sensitivity parameters and the real-time measurement data, the Levenberg-Marquardt method is applied for nonlinear least squares optimization to solve the system of equations Eq.(6). The optimal solution yields the TEP values.

When determining the initial values of variables R_{th} and

X_{th} , we first assume $|E_{th}|$ to be known, using $|\tilde{V}_k|$ as its approximate value. With $|E_{th}|$ fixed, the three-variable equations simplifies to two-variable equations, allowing us to solve for R_{th} and X_{th} as initial values (taking the real part of any complex solution). Subsequently, the three-variable equations is solved.

C. Method Advantages

The advantages of the proposed TEP identification method based on magnitude sensitivity are as follows:

- 1) **Use of Magnitude Sensitivity:** This method uses magnitude sensitivity for TEP identification, making it applicable to a wide range of power system equipment. It requires only basic measurement devices, which reduces costs. Compared to phase measurements, magnitude measurements provide higher accuracy, effectively reducing the impact of noise and system disturbances.
- 2) **Quick TEP Calculation:** With accurate magnitude sensitivity parameter identification, this method provides a fast tool for calculating TEP at any given moment. It uses sensitivity data to enable real-time assessment of the system's voltage support capabilities.
- 3) **No Extra Assumptions on Load Side:** This method relies only on Kirchhoff's laws and power definitions at the port, allowing for parameter identification at any time using measurement data. It aligns with the actual operating characteristics of power grids and, since it doesn't depend on specific load constraints, it is adaptable to diverse load conditions, offering high versatility.

The accuracy of the method largely depends on the precision of the magnitude sensitivity parameter identification. The next chapter focuses on the core issue of accurately identifying magnitude sensitivity parameters under the condition of stochastic fluctuations on the load side.

III. PRECISE SENSITIVITY IDENTIFICATION BASED ON STOCHASTIC RESPONSE STATISTICAL CHARACTERISTICS

For the scenario of load power stochastic fluctuations, the identification of port magnitude sensitivity parameters is performed. The corresponding port sensitivity relationship model, primarily includes three sections: power stochastic fluctuations, magnitude sensitivity relationship, and measurement errors, as shown in Fig. 2.

Power Random Fluctuations Section: The active power P and reactive power Q at the port exhibit stochastic fluctuations, which are modeled as a colored Gaussian process. This implies that the sample points are autocorrelated in a Gaussian process. Large-scale load fluctuations typically show strong correlation in the low-frequency range, indicating that slow changes (e.g., daily load variations) dominate. Therefore, these fluctuations can be treated as low-pass noise and can be simulated by passing white noise through a low-pass filter (e.g., Ornstein-Uhlenbeck (O-U) process). Furthermore, there may be cross-correlation between the stochastic fluctuations of P and Q .

Sensitivity Relationship Section: The stochastic fluctuations in load power data, after passing through the Thévenin

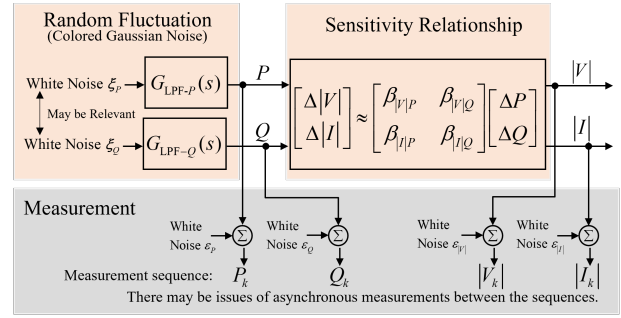


Fig. 2. Port magnitude sensitivity relationship under load power stochastic fluctuations.

equivalent system, can be approximated as a linear mapping through the magnitude sensitivity parameter matrix. This results in stochastic fluctuations in the port voltage magnitude $|V|$ and current magnitude $|I|$ around the operating point.

Measurement Section: The measurement processes of voltage magnitude, current magnitude, and power are all subject to measurement errors $\varepsilon_{|V|}$, $\varepsilon_{|I|}$, ε_P , ε_Q , which are assumed to follow Gaussian White Noise (GWN) characteristics. The noise is superimposed on the true values, resulting in fluctuating measurement data P_k , Q_k , $|V_k|$, $|I_k|$. Additionally, there may be issues related to asynchronous measurements between the electrical quantities.

A. Identification Based on Temporal Increments

For the sensitivity model shown in Fig. 2, the sensitivity parameters can be approximated using numerical differentiation methods, specifically through magnitude identification based on temporal increments [27], as shown as

$$\begin{bmatrix} |V_{k+1}| - |V_k| \\ |I_{k+1}| - |I_k| \end{bmatrix} \approx \begin{bmatrix} \beta_{|V|P} & \beta_{|V|Q} \\ \beta_{|I|P} & \beta_{|I|Q} \end{bmatrix} \begin{bmatrix} P_{k+1} - P_k \\ Q_{k+1} - Q_k \end{bmatrix} \quad (7)$$

where subscript $k = 1, 2, \dots, n$ denotes the k -th sampled data point. In this case, the actual data sequence used for identification is $Y_k = X_{k+1} - X_k$, $X = |V|, |I|, P, Q$. Based on Eq.(7), methods such as least squares fitting can be applied to obtain an approximation of the sensitivity parameters values.

In an ideal scenario, where no measurement errors or noise are present, the sensitivity identification method based on time-step increments provides high accuracy. However, measurement errors significantly impact the precision of the results. Even with large sample sizes, noise can increase uncertainty in parameter estimation.

When only environmental data is available, load fluctuations are typically small and stochastic, making the signal more susceptible to noise. This reduces the accuracy of sensitivity parameter identification, as noise interferes with meaningful fluctuation data. To extract valid information, a higher SNR may be needed to ensure the system characteristics reflect real signals rather than noise.

Therefore, improvements to the time-step increment-based sensitivity identification method are needed to mitigate low SNR effects, address parameter bias, and enhance robustness against stochastic disturbances.

B. Identification Based on Statistical Characteristics

1) Statistical Characteristics under Sliding Window

To extract the statistical characteristics of the time sequence of electrical quantities, the sliding window technique is applied to process the stochastic fluctuation data. By defining a sliding window, the time series is divided into smaller sub-windows, and statistical characteristics are calculated for each. As shown in Fig. 3, this approach generates a time-varying sequence of statistical characteristics, capturing the fluctuations of the statistical characteristics within each window.

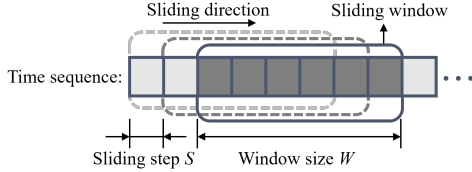


Fig. 3. Sliding window diagram. The window slides continuously along the data flow. The length of data within each window is called the window size W . The interval between adjacent window positions is the sliding step S .

Given the sampling period of the port electrical quantities as T_s , and to improve data utilization, the sliding step size is set as $S = T_s$. With the window size W , the number of data points within each sliding window is $n = WT_s^{-1}$, allowing for the acquisition of n measurements of the system's electrical quantities, denoted as $[X_k, X_{k+1}, \dots, X_{k+n-1}]$, $X = |V|, |I|, P, Q$.

When using statistical characteristics under the sliding window technique for sensitivity identification, each element of the new data sequence can be represented as

$$Y_k = f(X_k, X_{k+1}, \dots, X_{k+n-1}), X = |V|, |I|, P, Q$$

where f is the statistical function. When f is the mean function, the sample mean of the data within each sliding window is

$$\bar{X}_{w,k} = \frac{1}{n} \sum_{i=k}^{k+n-1} X_i, X = |V|, |I|, P, Q.$$

When f is the variance function, the sample variance of the data within each sliding window is

$$s_{X,k}^2 = \frac{1}{n-1} \sum_{i=k}^{k+n-1} (X_i - \bar{X}_{w,k})^2, X = |V|, |I|, P, Q.$$

Furthermore, considering the correlation between the stochastic fluctuations of active and reactive power, the sample covariance of P_k and Q_k within each sliding window is

$$s_{PQ,k} = \frac{1}{n-1} \sum_{i=k}^{k+n-1} [(P_i - \bar{P}_{w,k})(Q_i - \bar{Q}_{w,k})].$$

2) Mean-Based Identification under Sliding Window

From the time-incremental identification method shown in Eq.(7), we can further derive the sensitivity relationship based on the statistical characteristics of the temporal fluctuations.

First, the sensitivity relationship based on the mean within the sliding window can be derived. By summing the time-

incremental changes within the window, the same linear sensitivity relationship is maintained as

$$\begin{bmatrix} \sum_{j=k}^{k+n-1} (|V_j| - |V_j|) \\ \sum_{j=k}^{k+n-1} (|I_j| - |I_j|) \end{bmatrix} \approx \begin{bmatrix} \beta_{|V|P} & \beta_{|V|Q} \\ \beta_{|I|P} & \beta_{|I|Q} \end{bmatrix} \begin{bmatrix} \sum_{j=k}^{k+n-1} (P_k - P_j) \\ \sum_{j=k}^{k+n-1} (Q_k - Q_j) \end{bmatrix}. \quad (8)$$

From Eq.(8), we can derive the sensitivity identification method based on the window mean, as shown as

$$\begin{bmatrix} |V_k| - \bar{V}_{w,k} \\ |I_k| - \bar{I}_{w,k} \end{bmatrix} \approx \begin{bmatrix} \beta_{|V|P} & \beta_{|V|Q} \\ \beta_{|I|P} & \beta_{|I|Q} \end{bmatrix} \begin{bmatrix} P_k - \bar{P}_{w,k} \\ Q_k - \bar{Q}_{w,k} \end{bmatrix}. \quad (9)$$

In Eq.(9), the data sequence of statistical characteristics under the sliding window is $Y_k = X_k - \bar{X}_{w,k}$, $X = |V|, |I|, P, Q$.

3) Variance-Based Identification under Sliding Window

Furthermore, the sensitivity relationship based on the variance within the sliding window can be derived. By squaring and summing the deviations of the instantaneous values from the mean within the window in Eq.(9), a similar linear sensitivity relationship is obtained as

$$\begin{bmatrix} \sum_{j=k}^{k+n-1} (|V_j| - \bar{V}_{w,k})^2 \\ \sum_{j=k}^{k+n-1} (|I_j| - \bar{I}_{w,k})^2 \end{bmatrix} \approx \beta \begin{bmatrix} \sum_{j=k}^{k+n-1} (P_j - \bar{P}_{w,k})^2 \\ \sum_{j=k}^{k+n-1} (Q_j - \bar{Q}_{w,k})^2 \\ \sum_{j=k}^{k+n-1} [(P_j - \bar{P}_{w,k})(Q_j - \bar{Q}_{w,k})] \end{bmatrix}, \quad (10)$$

$$\beta = \begin{bmatrix} \beta_{|V|P}^2 & \beta_{|V|Q}^2 & 2\beta_{|V|P}\beta_{|V|Q} \\ \beta_{|I|P}^2 & \beta_{|I|Q}^2 & 2\beta_{|I|P}\beta_{|I|Q} \end{bmatrix}.$$

Eq.(10) can be transformed into a linear relationship between the electrical quantity sample variances and sample covariances. The sensitivity identification method based on the window variance is then given as

$$\begin{bmatrix} s_{|V|,k}^2 \\ s_{|I|,k}^2 \end{bmatrix} \approx \begin{bmatrix} \beta_{|V|P}^2 & \beta_{|V|Q}^2 & 2\beta_{|V|P}\beta_{|V|Q} \\ \beta_{|I|P}^2 & \beta_{|I|Q}^2 & 2\beta_{|I|P}\beta_{|I|Q} \end{bmatrix} \begin{bmatrix} s_{P,k}^2 \\ s_{Q,k}^2 \\ s_{PQ,k} \end{bmatrix} + \begin{bmatrix} \mu_{\epsilon_1} \\ \mu_{\epsilon_2} \end{bmatrix}. \quad (11)$$

In Eq.(11), μ_{ϵ_1} and μ_{ϵ_2} represent the expected values of the identification errors, which arise from measurement errors in the electrical quantities. As shown in Fig. 2, the measurement errors are modeled as zero-mean GWN. Consequently, the error terms in Eq.(7) and Eq.(9) have an expected value of zero, while the error term in Eq.(11) reflects the variance of the measurement noise, which is non-zero. Therefore, Eq.(11) should include constant terms μ_{ϵ_1} , μ_{ϵ_2} equal to the expected value of the errors. When the fluctuations of active power and reactive power are cross-correlated, $s_{PQ,k} \neq 0$. Eq.(11) reflects the relationship between the sample variance of electrical quantities under the sliding window and the sensitivity parameters. In Eq.(11), the data sequence of statistical characteristics under the sliding window Y_k is $s_{PQ,k}$ and $s_{X,k}^2$, $X = |V|, |I|, P, Q$.

C. Comparison of Identification Methods Performance

This section compares the sensitivity identification methods based on temporal increments (Eq.(7)), windowed mean (Eq.(9)), and windowed variance (Eq.(11)). Theoretical analysis will be conducted to evaluate their performance in terms

of improvements in SNR, robustness against asynchronous measurements, and handling of data collinearity.

1) Improvement in SNR

In power systems, stochastic disturbances in electrical quantities that vary over time can be treated as a stationary stochastic process, considering both their temporal changes and mutual correlations. For a stationary Gaussian stochastic process $X(t)$, the autocovariance function $R_X(\tau) = \text{cov}[X(t), X(t+\tau)]$, characterizes the covariance of $X(t)$ at different time instances. τ indicates the time difference.

The value of the autocovariance function $R_X(\tau)$ at $\tau = 0$ is equal to the variance of the process σ_X^2 . By normalizing the autocovariance function using σ_X^2 , the normalized autocovariance function is obtained as $\rho(\tau) = R_X(\tau)/\sigma_X^2$.

$\rho(\tau)$ of a stationary Gaussian process is an even function, typically peaking at 1 when $\tau = 0$. For low-pass Gaussian colored noise, $\rho(\tau)$ decays or oscillates as t increases. The time required for the autocovariance function to decay to e^{-1} times its initial value is defined as the autocovariance time constant τ_c .

In a sliding window with uniform sampling at a fixed interval T_s , the n stochastic samples at n time steps form an n -dimensional stochastic variable $\mathbf{X} = [X_1, X_2, \dots, X_n]^T$. When the system state remains stable, these stochastic variables follow the same probability distribution and exhibit the same statistical characteristics. Due to the temporal correlation in the electrical quantity sequences of power systems, \mathbf{X} exhibits correlation.

The covariance matrix of \mathbf{X} is denoted as \mathbf{C}_X . Since the elements of the matrix satisfy $C_{X(i,j)} = C_{X(j,i)} = \text{cov}(X_i, X_j)$, $i, j = 1, 2, \dots, n$, \mathbf{C}_X is symmetric and Toeplitz. The relationship between the covariance matrix and the autocovariance function is

$$\mathbf{C}_X = \sigma_X^2 \begin{bmatrix} 1 & \rho(T_s) & \dots & \rho((n-1)T_s) \\ \rho(T_s) & 1 & \dots & \rho((n-2)T_s) \\ \vdots & \vdots & \ddots & \vdots \\ \rho((n-1)T_s) & \rho((n-2)T_s) & \dots & 1 \end{bmatrix}.$$

Due to the decaying or oscillatory nature of the first row in the Toeplitz matrix, the row or column sums are typically largest in the middle rows and smallest at the boundaries.

The measurement errors $\varepsilon(t)$ is zero-mean GWN with variance σ_ε^2 . After applying the sliding window, $\varepsilon(t)$ also becomes an n -dimensional stochastic variable, with independent components, each following a zero-mean Gaussian distribution. Therefore, the covariance matrix has σ_ε^2 on the diagonal and zeros elsewhere.

Since both the signal and system noise are stochastic variables, the system SNR is defined using variance to quantify the signal's effectiveness relative to the noise strength, as

$$\text{SNR}_0 \text{ (dB)} = 10 \log_{10} \left[\frac{\text{var}(X)}{\text{var}(\varepsilon)} \right] = 10 \log_{10} \left[\frac{\sigma_X^2}{\sigma_\varepsilon^2} \right]. \quad (12)$$

The following compares the SNR of the data used in the three identification methods. The theoretical variance of the temporal increments sequence $Y_k = X_{k+1} - X_k$ is

$$\text{var}(X_{k+1} - X_k) = 2\sigma_X^2(1 - \rho(T_s)). \quad (13)$$

The theoretical variance of the temporal increments sequence of the measurement error $\text{var}(\varepsilon_{k+1} - \varepsilon_k)$ is $2\sigma_\varepsilon^2$. Therefore, when calculating the sensitivity based on temporal increments, the theoretical value of the SNR for the data is

$$\text{SNR}_1 = \text{SNR}_0 + 10 \log_{10}(1 - \rho(T_s)). \quad (14)$$

When $T_s \ll \tau_c$, $\rho(T_s) \approx 1$. The data's SNR significantly decreases, which severely affects the accuracy of the least squares identification results.

For identification based on statistical characteristics under the sliding window, the statistical characteristics (such as sample mean, sample variance, and sample covariance) are also stochastic variables.

The theoretical variance of the data sequence used by mean-based identification $Y_k = X_k - \bar{X}_{w,k}$, is

$$\begin{aligned} \text{var}(X_k - \bar{X}_{w,k}) &= C_{X(1,1)} - \frac{2}{n} \sum_{j=1}^n C_{X(1,j)} \\ &\quad + \frac{1}{n^2} \sum_{i=1}^n \sum_{j=1}^n C_{X(i,j)}. \end{aligned} \quad (15)$$

When $W \gg \tau_c \gg T_s$, the variance can be quickly approximated as

$$\text{var}(X_k - \bar{X}_{w,k}) \approx \sigma_X^2 \left(1 - \frac{2}{nT_s} \int_{-nT_s/2}^{nT_s/2} \rho(\tau) d\tau \right) \approx \sigma_X^2. \quad (16)$$

The data sequence of measurement noise is $\varepsilon_k - \bar{\varepsilon}_w$, and its theoretical variance can be considered as a special case of Eq.(15), given as $\frac{n-1}{n} \sigma_\varepsilon^2$. Therefore, when calculating the sensitivity based on sample mean under the sliding window, $\text{SNR}_2 \approx \text{SNR}_0$.

The data sequence used by variance-based identification is $s_{X,k}^2$ and $s_{PQ,k}$. Assuming that the PQ measurement noises are independent, thus the SNR related to the covariance $s_{PQ,k}$ is not a concern. The theoretical variance of $s_{X,k}^2$ is

$$\text{var}(s_{X,k}^2) = \frac{2}{(n-1)^2} \left(S_{1a} - \frac{2}{n} S_{2a} + \frac{1}{n^2} S_{3a} \right) \quad (17)$$

where $S_{1a} = \sum_{i=1}^n \sum_{j=1}^n C_{X(i,j)}^2$, $S_{2a} = \sum_{i=1}^n \left(\sum_{j=1}^n C_{X(i,j)} \right)^2$, $S_{3a} = \left(\sum_{i=1}^n \sum_{j=1}^n C_{X(i,j)} \right)^2$. When $W \gg \tau_c \gg T_s$, the variance of $s_{X,k}^2$ can be quickly approximated as

$$\text{var}(s_{X,k}^2) \approx \frac{2\sigma_X^4}{(n-1)T_s} \int_{-nT_s/2}^{nT_s/2} \rho(\tau)^2 d\tau. \quad (18)$$

The data sequence of measurement noise s_ε^2 follows a chi-square distribution. Its theoretical variance can be considered as a special case of Eq.(17), given as $\frac{2}{n-1} \sigma_\varepsilon^4$. Therefore, when calculating the sensitivity based on sample variance under the sliding window,

$$\text{SNR}_3 \approx 2\text{SNR}_0 + 10 \log_{10} \left[\frac{1}{T_s} \int_{-nT_s/2}^{nT_s/2} \rho_X(\tau)^2 d\tau \right]. \quad (19)$$

The integral term measures the correlation strength of $X(t)$ within interval $\tau \in [-nT_s/2, nT_s/2]$, capturing the variation of the autocovariance function over the interval.

As shown in Eq.(19), since the electrical signals are modeled as Gaussian colored noise, sensitivity identification using

sample variance and covariance within the sliding window can benefit from an increase in window size W or a reduction in the sampling period T_s . These adjustments effectively enhance the system's SNR, thereby improving the accuracy of the sensitivity identification.

For example, the random fluctuations of electrical quantities are modeled using an O-U process, with added GWN as measurement noise. The original data's SNR is set to 0 dB, meaning the variance of the random process signal is equal to that of the noise, indicating low data quality. The SNR for different identification methods is shown in Fig. 4.

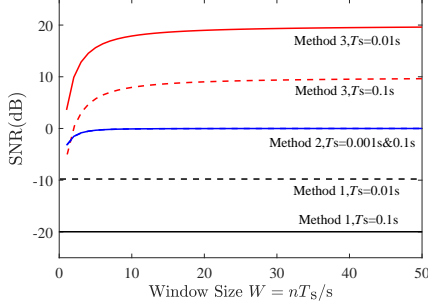


Fig. 4. Data SNR of different identification methods. Method 1 represents the temporal increments based identification. Method 2 represents the mean-based identification under sliding window. Method 3 represents the variance-based identification under sliding window. The O-U process has a mean-reversion coefficient of 1, a diffusion coefficient of $\sqrt{2}$, and a variance of 1. The variance of GWN is 1.

Fig. 4 shows that method based on stochastic characteristics performs well in improving the SNR, especially method 3. Even with low initial data SNR, sensitivity identification using the variance and covariance under the sliding window effectively improves the system's SNR.

2) Robustness under Asynchronous Measurements

When asynchronous measurement issues occur, assume a delay of m sampling periods, i.e., a time shift $\tau = mT_s$, $m > 0$. The theoretical value of the time increment data is Y_k , while the actual measurement is \tilde{Y}_k . The relative error can be quantified by the variance as

$$\epsilon_r = \frac{\text{var}(\tilde{Y}_k - Y_k)}{\text{var}(Y_k)} = 2 - \frac{2 \text{cov}(Y_k, \tilde{Y}_k)}{\text{var}(Y_k)}. \quad (20)$$

The following compares the relative error of three identification methods under asynchronous measurement conditions.

When calculating sensitivity using temporal increments, the covariance between the asynchronous measurement value $\tilde{Y}_k = X_{k+m+1} - X_{k+m}$ and the theoretical value $Y_k = X_{k+1} - X_k$ is $\text{cov}(Y_k, \tilde{Y}_k) = \sigma_X^2 [2\rho(mT_s) - \rho((m-1)T_s) - \rho((m+1)T_s)]$. Therefore, the relative error is given by

$$\epsilon_r = 2 - \frac{2\rho(mT_s) - \rho((m-1)T_s) - \rho((m+1)T_s)}{1 - \rho(T_s)}. \quad (21)$$

For identification based on statistical characteristics, the random samples at n time steps within the window can be treated as an n -dimensional random variable. The true values of the random variables are denoted as $\mathbf{X} =$

$[X_k, X_{k+1}, \dots, X_{k+n-1}]^T$, and the actual measured values are denoted as $\tilde{\mathbf{X}} = [X_{k+m}, X_{k+m+1}, \dots, X_{k+m+n-1}]^T$. The covariance matrix between \mathbf{X} and $\tilde{\mathbf{X}}$ is denoted as $\tilde{\mathbf{C}}_{\mathbf{X}}$. Since the elements of the matrix satisfy $\tilde{C}_{\mathbf{X}}(i,j) = \text{cov}(X_{k+i-1}, X_{k+m+j-1})$, $i, j = 1, 2, \dots, n$, $\tilde{\mathbf{C}}_{\mathbf{X}}$ is no longer a symmetric Toeplitz matrix. The relationship between $\tilde{\mathbf{C}}_{\mathbf{X}}$ and the autocovariance function is given by

$$\tilde{\mathbf{C}}_{\mathbf{X}} = \sigma_X^2 \begin{bmatrix} \rho(mT_s) & \rho((m+1)T_s) & \dots & \rho((m+n-1)T_s) \\ \rho((m-1)T_s) & \rho(mT_s) & \dots & \rho((m+n-2)T_s) \\ \vdots & \vdots & \ddots & \vdots \\ \rho((m-n+1)T_s) & \rho((m-n+2)T_s) & \dots & \rho(mT_s) \end{bmatrix}.$$

For identification based on statistical characteristics under the sliding window, the theoretical value of the data in each sliding window is $Y_k = f(X_k, X_{k+1}, \dots, X_{k+n-1})$, while the actual measured value is $\tilde{Y}_k = Y_{k+m} = f(X_{k+m}, X_{k+m+1}, \dots, X_{k+m+n-1})$.

For mean-based identification, the theoretical value for each sliding window is $Y_k = X_k - \bar{X}_{w,k}$, and the actual measured value should be $\tilde{Y}_k = Y_{k+m}$. The covariance between Y_k and \tilde{Y}_k is given by

$$\text{cov}(Y_k, \tilde{Y}_k) = \tilde{C}_{\mathbf{X}}(1,1) - \frac{1}{n} \sum_{i=1}^n \tilde{C}_{\mathbf{X}}(i,1) - \frac{1}{n} \sum_{j=1}^n \tilde{C}_{\mathbf{X}}(1,j) + \frac{1}{n^2} \sum_{i=1}^n \sum_{j=1}^n \tilde{C}_{\mathbf{X}}(i,j). \quad (22)$$

For variance-based identification, the theoretical value for each sliding window is $Y_k = s_{X,k}^2$, and the actual measured value should be $\tilde{Y}_k = Y_{k+m} = s_{X,k+m}^2$. The covariance between Y_k and \tilde{Y}_k is given by

$$\text{cov}(Y_k, \tilde{Y}_k) = \frac{2}{(n-1)^2} (S_{1b} - \frac{1}{n} S_{2b} - \frac{1}{n} S_{3b} + \frac{1}{n^2} S_{4b}) \quad (23)$$

where $S_{1b} = \sum_{i,j=1}^n \tilde{C}_{\mathbf{X}}^2(i,j)$, $S_{2b} = \sum_{i=1}^n (\sum_{j=1}^n \tilde{C}_{\mathbf{X}}(i,j))^2$, $S_{3b} = \sum_{j=1}^n (\sum_{i=1}^n \tilde{C}_{\mathbf{X}}(i,j))^2$, $S_{4b} = (\sum_{i=1}^n \sum_{j=1}^n \tilde{C}_{\mathbf{X}}(i,j))^2$.

Taking the O-U process as an example, when asynchronous measurement issues occur in the signal, the relative error for different identification methods is shown in Fig. 5.

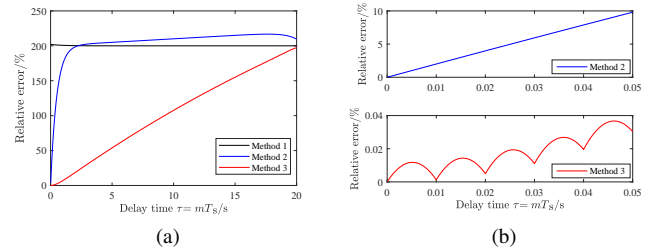


Fig. 5. Data relative error of different identification methods. (a) τ is an integer multiple of T_s . (b) τ is a non-integer multiple of T_s . Method 1 represents the temporal increments based identification. Method 2 represents the mean-based identification under sliding window. Method 3 represents the variance-based identification under sliding window. O-U process parameters are the same as those in Fig. 4. The sampling period is $T_s = 0.01$ s, and the sliding window length is $W = 20$ s.

Fig. 5 demonstrates the excellent robustness of the method based on stochastic characteristics under asynchronous measurements, especially method 3. Even in the presence of time delays in asynchronous measurement signals, sensitivity identification using the variance and covariance under the sliding

window can still provide accurate estimates, demonstrating the method's robustness against measurement inconsistencies.

3) Handling of Data Collinearity

The active and reactive power data may exhibit bivariate collinearity (the power correlation is modeled according to [28]). Let the correlation coefficient between the measured power data be denoted as $\text{corr}(P_k, Q_k) = r_{PQ}$, where $0 \leq r_{PQ} \leq 1$, and assume that the variances σ_P^2 and σ_Q^2 are equal. The condition numbers of the power data for each identification method can be computed to assess the robustness of the method under such collinearity.

When the $n \times m$ random matrix \mathbf{A} is composed of m correlated random variables' measurement data column vectors, which follow Gaussian distribution. Matrix \mathbf{A}_{dec} is obtained by centering \mathbf{A} using the column means $\mu = [\mu_1, \mu_2, \dots, \mu_n]$. The condition number $\kappa(\mathbf{A}_{\text{dec}})$ is the ratio of the largest to smallest singular value of \mathbf{A}_{dec} , depending on the correlation between different columns of \mathbf{A}_{dec} .

The squared singular values σ_i^2 of matrix \mathbf{A}_{dec} are equal to the eigenvalues λ_i of matrix $\mathbf{A}_{\text{dec}}^T \mathbf{A}_{\text{dec}}$. Thus, the square of $\kappa(\mathbf{A}_{\text{dec}})$ equals the condition number of the covariance matrix $\text{cov}(\mathbf{A}) = \frac{1}{n-1} \mathbf{A}_{\text{dec}}^T \mathbf{A}_{\text{dec}}$ [29]. When the m column random fluctuations have equal variance, the square of $\kappa(\mathbf{A}_{\text{dec}})$ equals the condition number of the correlation matrix $\text{corr}(\mathbf{A}_{\text{dec}})$.

When calculating sensitivity using temporal increments, the covariance between $P_{k+1} - P_k$ and $Q_{k+1} - Q_k$ is

$$\text{cov}(P_{k+1} - P_k, Q_{k+1} - Q_k) = 2r_{PQ}\sigma_P\sigma_Q(1 - \rho(T_s)) \quad (24)$$

Combining Eq.(13) and Eq.(24), the correlation coefficient matrix of $\mathbf{A} = [P_{k+1} - P_k, Q_{k+1} - Q_k]$ is given by

$$\text{corr}(\mathbf{A}) = \begin{bmatrix} 1 & r_{PQ} \\ r_{PQ} & 1 \end{bmatrix}. \quad (25)$$

The theoretical condition number of \mathbf{A}_{dec} is

$$\kappa_1(\mathbf{A}_{\text{dec}}) = \sqrt{\frac{1 + r_{PQ}}{1 - r_{PQ}}}. \quad (26)$$

When using statistical characteristics for identification, the power stochastic variables under the sliding window are denoted as $\mathbf{P} = [P_k, P_{k+1}, \dots, P_{k+n-1}]^T$ and $\mathbf{Q} = [Q_k, Q_{k+1}, \dots, Q_{k+n-1}]^T$. The values between \mathbf{P} and \mathbf{Q} is denoted as C_{PQ} . According to the modeling method in [28], when the normalized autocovariance functions $\rho_P(\tau)$ and $\rho_Q(\tau)$ are identical, the normalized cross-covariance function between \mathbf{P} and \mathbf{Q} is the same as $\rho_P(\tau)$ and $\rho_Q(\tau)$. Therefore, the relationship between C_{PQ} and the autocovariance function is given by

$$C_{PQ} = r_{PQ}\sigma_P\sigma_Q \begin{bmatrix} 1 & \rho(T_s) & \dots & \rho((n-1)T_s) \\ \rho(T_s) & 1 & \dots & \rho((n-2)T_s) \\ \vdots & \vdots & \ddots & \vdots \\ \rho((n-1)T_s) & \rho((n-2)T_s) & \dots & 1 \end{bmatrix}.$$

For mean-based identification, the covariance between $P_k - \bar{P}_{w,k}$ and $Q_k - \bar{Q}_{w,k}$ is given by

$$\text{cov}(P_k - \bar{P}_{w,k}, Q_k - \bar{Q}_{w,k}) = C_{PQ(1,1)} - \frac{2}{n} \sum_{i=1}^n C_{PQ(i,1)} + \frac{1}{n^2} \sum_{i,j=1}^n C_{PQ(i,j)}. \quad (27)$$

Combining Eq.(15) and Eq.(27), the correlation coefficient matrix of $\mathbf{A} = [P_k - \bar{P}_{w,k}, Q_k - \bar{Q}_{w,k}]$ is the same as Eq.(25). The theoretical condition number of \mathbf{A}_{dec} is the same as Eq.(26).

For variance-based identification, the covariance between $s_{P,k}^2$ and $s_{Q,k}^2$ is given by

$$\text{cov}(s_{P,k}^2, s_{Q,k}^2) = \frac{2}{(n-1)^2} \left(S_{1c} - \frac{2}{n} S_{2c} + \frac{1}{n^2} S_{3c} \right) \quad (28)$$

where $S_{1c} = \sum_{i=1}^n C_{PQ(i,j)}^2$, $S_{2c} = \sum_{i=1}^n \left(\sum_{j=1}^n C_{PQ(i,j)} \right)^2$, $S_{3c} = \left(\sum_{i=1}^n \sum_{j=1}^n C_{PQ(i,j)} \right)^2$. The covariance between $s_{P,k}^2$ and $s_{PQ,k}$, and between $s_{Q,k}^2$ and $s_{PQ,k}$ is given by

$$\text{cov}(s_{X,k}^2, s_{PQ,k}) = \frac{2}{(n-1)^2} \left(S_{1d} - \frac{2}{n} S_{2d} + \frac{1}{n^2} S_{3d} \right) \quad (29)$$

where $S_{1d} = \sum_{i=1}^n \sum_{j=1}^n (C_{X(i,j)} C_{PQ(i,j)})$,

$$S_{2d} = \sum_{i=1}^n \left(\sum_{j=1}^n C_{X(i,j)} \sum_{j=1}^n C_{PQ(i,j)} \right),$$

$$S_{3d} = \sum_{i=1}^n \sum_{j=1}^n C_{X(i,j)} \sum_{i=1}^n \sum_{j=1}^n C_{PQ(i,j)}, \quad X = P, Q.$$

The variance of $s_{PQ,k}$ is given by

$$\text{var}(s_{PQ,k}) = \frac{2}{(n-1)^2} \left(S_{1e} - \frac{1}{n} S_{2e} + \frac{1}{n^2} S_{3e} \right). \quad (30)$$

where $S_{1e} = \sum_{i=1}^n \sum_{j=1}^n (C_{P(i,j)} C_{Q(i,j)}) + \sum_{i=1}^n \sum_{j=1}^n C_{PQ(i,j)}^2$,

$$S_{2e} = \sum_{i=1}^n \sum_{j=1}^n C_{P(i,j)} \sum_{i=1}^n \sum_{j=1}^n C_{Q(i,j)} + \left(\sum_{i,j=1}^n C_{PQ(i,j)} \right)^2,$$

$S_{3e} = \sum_{i=1}^n \left[\sum_{j=1}^n C_{P(i,j)} \sum_{j=1}^n C_{Q(i,j)} + \left(\sum_{j=1}^n C_{PQ(i,j)} \right)^2 \right]$. Combining Eq.(17) and Eq.(28)-Eq.(30), the correlation coefficient matrix of $\mathbf{A} = [s_{P,k}^2, s_{Q,k}^2, s_{PQ,k}]$ is

$$\text{corr}(\mathbf{A}) = \begin{bmatrix} 1 & r_{PQ}^2 & \sqrt{\frac{2}{1+r_{PQ}^2}} r_{PQ} \\ r_{PQ}^2 & 1 & \sqrt{\frac{2}{1+r_{PQ}^2}} r_{PQ} \\ \sqrt{\frac{2}{1+r_{PQ}^2}} r_{PQ} & \sqrt{\frac{2}{1+r_{PQ}^2}} r_{PQ} & 1 \end{bmatrix}. \quad (31)$$

The theoretical condition number of \mathbf{A}_{dec} is

$$\kappa_3(\mathbf{A}_{\text{dec}}) = \sqrt{\frac{\sqrt{r_{PQ}^2+1}(r_{PQ}^2+2)+r_{PQ}\sqrt{r_{PQ}^4+r_{PQ}^2+16}}{\sqrt{r_{PQ}^2+1}(r_{PQ}^2+2)-r_{PQ}\sqrt{r_{PQ}^4+r_{PQ}^2+16}}}. \quad (32)$$

The theoretical condition number of the data matrix based on different identification methods is shown in Fig. 6, with variations in data correlation.

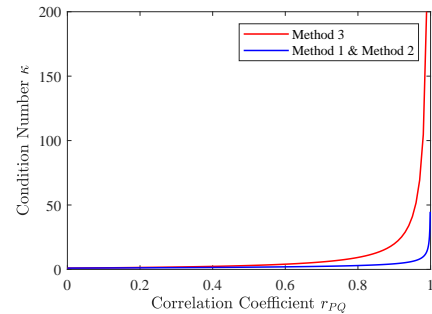


Fig. 6. Condition numbers of different identification methods. Method 1 represents the temporal increments based identification. Method 2 represents the mean-based identification under sliding window. Method 3 represents the variance-based identification under sliding window.

As shown in Fig. 6, when the correlation of P_k and Q_k is low, the identification methods based on mean and variance do not significantly exacerbate the data collinearity. However, when correlation is extremely high, the variance-based method leads to a noticeable increase in data collinearity. The effectiveness of identification methods in addressing low SNR, asynchronous measurements, and data collinearity is interrelated. Therefore, relying solely on differences in a single dimension is insufficient to assert that one method is inherently inferior to others; a comprehensive evaluation is required to assess their overall performance.

4) Optimal Method Selection

The error in sensitivity identification results is influenced by a combination of the SNR, asynchronous measurements, and data collinearity. Qualitatively, when the SNR is low or asynchronous measurements are present, variance-based method should be applied. In cases where there is significant collinearity between power variables, mean-based is more suitable for identification.

Sensitivity identification can be regarded as an $\mathbf{Ax} = \mathbf{b}$ type identification. The data and identification objectives for different identification methods are shown in Table I.

TABLE I
DATA AND IDENTIFICATION OBJECTIVES OF
DIFFERENT IDENTIFICATION METHODS

Method	\mathbf{A}	\mathbf{x}	\mathbf{b}
Temporal Increments Based	$\begin{bmatrix} P_{k+1} - P_k \\ Q_{k+1} - Q_k \end{bmatrix}^T$	$\begin{bmatrix} \beta_{ V P} & \beta_{ I P} \\ \beta_{ V Q} & \beta_{ I Q} \end{bmatrix}$	$\begin{bmatrix} V_{k+1} - V_k \\ I_{k+1} - I_k \end{bmatrix}^T$
Mean Based	$\begin{bmatrix} P_k - \bar{P}_{w,k} \\ Q_k - \bar{Q}_{w,k} \end{bmatrix}^T$	$\begin{bmatrix} \beta_{ V P} & \beta_{ I P} \\ \beta_{ V Q} & \beta_{ I Q} \end{bmatrix}$	$\begin{bmatrix} V_k - \bar{V}_{w,k} \\ I_k - \bar{I}_{w,k} \end{bmatrix}^T$
Variance Based	$\begin{bmatrix} s_{P,k}^2 \\ s_{Q,k}^2 \\ s_{PQ,k} \end{bmatrix}^T$	$\begin{bmatrix} \beta_{ V P}^2 & \beta_{ I P}^2 \\ \beta_{ V Q}^2 & \beta_{ I Q}^2 \\ 2\beta_{ V P}\beta_{ V Q} & 2\beta_{ I P}\beta_{ I Q} \end{bmatrix}$	$\begin{bmatrix} s_{ V ,k}^2 \\ s_{ I ,k}^2 \end{bmatrix}^T$

Due to the varying expectations of data in different sensitivity identification methods, decentralization must be applied before calculating the error bound. According to the law of large numbers, with a sufficiently large sample size, the sample mean approximates the expected value. Decentralizing the data eliminates mean shifts, ensuring that the accuracy of identification results depends solely on the method, rather than on data magnitude or units.

In the quantitative analysis of identification result errors, the error bound can be effectively controlled through the condition number inequality applied to the decentralized data, as

$$\frac{\|\hat{\mathbf{x}} - \mathbf{x}\|_F}{\|\mathbf{x}\|_F} \leq \kappa(\mathbf{A}_{\text{dec}}) \left(\frac{\|\hat{\mathbf{A}}_{\text{dec}} - \mathbf{A}_{\text{dec}}\|_F}{\|\mathbf{A}_{\text{dec}}\|_F} + \frac{\|\hat{\mathbf{b}}_{\text{dec}} - \mathbf{b}_{\text{dec}}\|_F}{\|\mathbf{b}_{\text{dec}}\|_F} \right) \quad (33)$$

where, $\|\cdot\|_F$ represents the Frobenius norm (F-norm). The F-norm of a decentralized random sequence is proportional to the variance of the sequence. $\hat{\mathbf{x}}$ denotes the estimated value of the sensitivity parameters \mathbf{x} . $\hat{\mathbf{A}}_{\text{dec}}$ and $\hat{\mathbf{b}}_{\text{dec}}$ represents the actual measured value of \mathbf{A} and \mathbf{b} after decentralization, respectively.

The SNR improvement and the relative error under asynchronous measurements are related to the F-norms of the matrices \mathbf{A} and \mathbf{b} . The condition number $\kappa(\mathbf{A}_{\text{dec}})$ is positively correlated with the correlation coefficients within the matrix \mathbf{A} . Based on the condition number inequality, the error upper

bound of the solution in each method can be estimated. By comparing these error bounds, the optimal method for a specific data condition can be selected.

D. Selection of Sliding Window Parameters

For the identification method based on statistical characteristics with a sliding window, the window size W and sliding step S are key factors affecting both computational accuracy and efficiency. W determines the number of data elements in the window, while S controls the overlap of data between consecutive windows.

For the sliding step S , to maximize data utilization and enhance robustness, S is typically set to T_s , allowing the window to move one step at a time.

For the window size W , the goal is to optimize the method's performance in improving SNR. As shown in Fig. 4, while longer windows can enhance estimation accuracy, it is also crucial to reduce the data load required for each calculation to enhance computational efficiency. First, the autocovariance function of the signal is estimated and converted into a covariance matrix. Using equation (21), the SNR improvement is evaluated for different window lengths. In practice, W is typically chosen based on the signal's autocovariance decay time constant τ_c , setting $W = 5\tau_c \sim 10\tau_c$. If the identification results do not converge, W can be further increased or the sampling period T_s of the system can be reduced.

IV. SIMULATION VERIFICATION

A. Simulation Validation of Method Effectiveness

1) Case Setup

The case model used for the simulation is shown in Fig. 1. The simulation is conducted in the MATLAB environment. The test case parameters are as follows: the source voltage is $E = 270$ kV, the impedance is $Z = R + jX = (50 + j50) \Omega$. The active and reactive power of the stochastic load are defined by a bivariate correlated O-U process [28] as

$$\begin{cases} P(t) = (P_0 + \eta_P(t)) (|V|(t) / |V_0|)^{\gamma_P} \\ Q(t) = (Q_0 + \eta_Q(t)) (|V|(t) / |V_0|)^{\gamma_Q} \\ \dot{\eta}_P(t) = -\alpha_P \eta_P(t) + b_P \xi_P(t) \\ \dot{\eta}_Q(t) = -\alpha_Q \eta_Q(t) + b_Q (r_{PQ} \xi_P(t) + \sqrt{1 - r_{PQ}^2} \xi_Q(t)) \end{cases} \quad (34)$$

where the mathematical expectations of power are $P_0 = 50$ MW and $Q_0 = 50$ MVar, $|V|(t)$ is the magnitude of the bus voltage at the load side, $|V_0|$ is the initial value of the voltage magnitude at time $t = 0$. γ_P and γ_Q represent the voltage-power correlation at the load side. $\gamma_P = \gamma_Q = 0$ indicates a constant power load, and $\gamma_P = \gamma_Q = 2$ indicates a constant impedance load."

$\eta_P(t)$ and $\eta_Q(t)$ are modeled as bivariate correlated zero-mean O-U processes. The drift term is $\alpha_P = \alpha_Q = 1$. The diffusion term is $b_P = b_Q = \sqrt{2}$. The variance is $\sigma_{\eta_P}^2 = \sigma_{\eta_Q}^2 = 1$. $\xi_P(t)$ and $\xi_Q(t)$ are independent standard GWN, with parameter r_{PQ} indicating their correlation. When $r_{PQ} = 0$, the fluctuations in active and reactive power are uncorrelated.

2) Effectiveness for Various Load Types

To verify the applicability and accuracy of the proposed TEP identification method under different load types, simulations were conducted using two typical load types, constant power load and constant impedance load. The performance of the proposed method under varying load conditions was evaluated through simulation comparisons.

In addition to the proposed method, we also compares the ordinary least squares method, ridge regression [24], [25], and total least squares from [23], to evaluate the performance of different methods in TEP identification. The violin plot in Fig. 7 presents the probability distribution of TEP identification results for each method, providing an intuitive comparison of the identification accuracy and stability under different load types conditions.

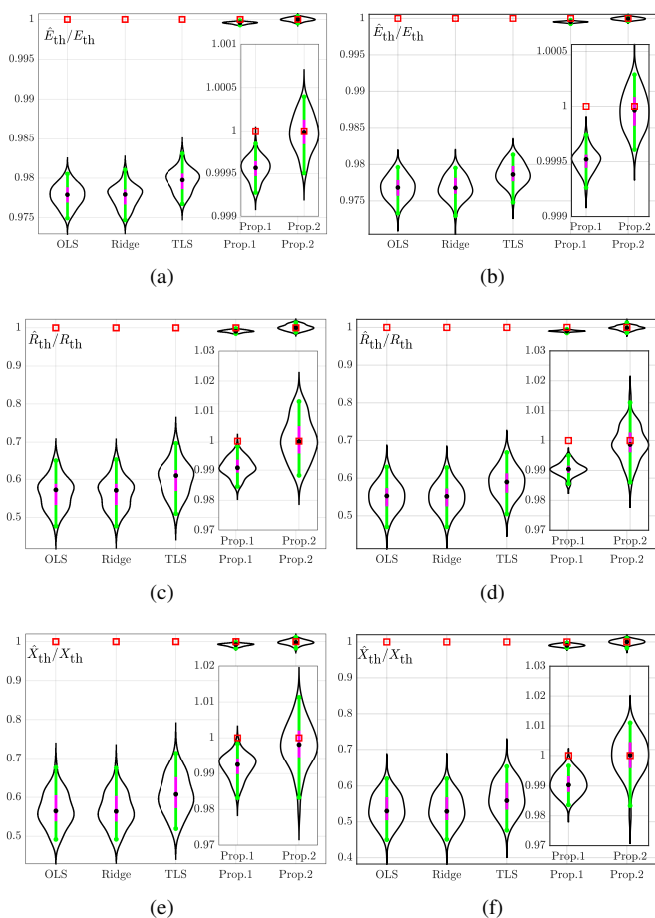


Fig. 7. Violin plots of TEP identification results. (a), (c), (e) with constant power load. (b), (d), (f) with constant impedance load. In the violin plots, the black solid line contour illustrates the probability distribution of results from each method (obtained via kernel density estimation), and the red box represents the theoretical true values of the parameters. The black solid circle marks the median of the identification results, while the hollow square represents the theoretical values. The magenta bar indicates the interquartile range (IQR), i.e., the difference between the 75th and 25th percentiles of the data. The green solid circles represent the nearest upper and lower bound values, which are the maximum observation less than or equal to the third quartile plus $1.5 \times \text{IQR}$ and the minimum observation greater than or equal to the first quartile minus $1.5 \times \text{IQR}$, respectively.

In Fig. 7, the horizontal axis represents the different methods employed, including literature methods (OLS, Ridge, TLS)

and the proposed methods (Prop.1 mean-based and Prop.2 variance-based). The correlation coefficients $r_{PQ} = 0.2$. The noise variance in electrical quantities $|V|$, $|I|$, P , Q , are set to 1% of the signal variance, corresponding to a SNR of 20 dB. The simulation was performed with 50 independent Monte Carlo experiments, each simulating for 2 minutes. The sampling period $T_s = 0.01$ s and the sliding window size $W = 5$ s.

The inset zoom of Fig. 7 provides a closer look at the distribution of results from the proposed methods (Prop.1 mean-based and Prop.2 variance-based), enabling a more precise comparison of their accuracy and bias. The simulation results show that, for different load types, the TEP identification using the proposed methods based on stochastic characteristics maintains strong unbiasedness and stability. Compared to methods in the literature, the proposed methods' estimates, with median values (black solid points in Fig. 7) closely matching the theoretical values (empty square markers), confirm their unbiased nature. Additionally, the narrow interquartile range (IQR) (magenta vertical bars) and the deviation between adjacent values (green solid points) and the median, within 2%, further validate the methods' consistent stability.

3) Effectiveness under Low SNR

To further assess the effectiveness of the proposed method under low SNR conditions, we reduce the SNR in the simulation and compare the results with literature methods. Figure 8 shows the violin plots of the different methods under low SNR conditions. The simulation results in Fig. 8 show that, despite the reduced SNR, the proposed method consistently maintains high TEP identification accuracy, further confirming its robustness and advantages in noisy environments.

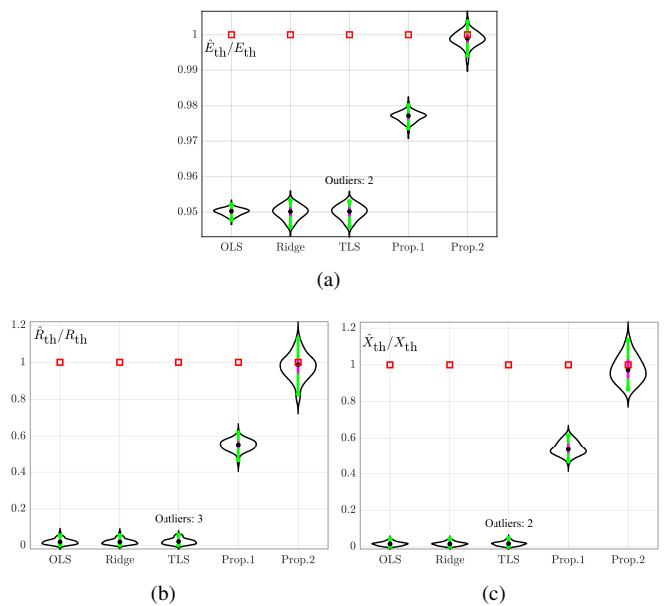


Fig. 8. Violin plots of TEP identification results under low SNR conditions. The load type is a constant power load. $r_{PQ} = 0.2$. The noise variance in the electrical quantities is equal to the signal variance, resulting in a SNR of 0 dB. A Monte Carlo experiment is conducted with simulation parameters identical to those in Fig. 7.

4) Effectiveness under Asynchronous Measurements

To further validate the effectiveness of the proposed method under asynchronous measurements, we introduced a 0.05s delay between current and voltage measurements, simulating time misalignment due to asynchronous measurements or data transmission delays. Figure 10 shows the violin plots of the methods under asynchronous measurement conditions.

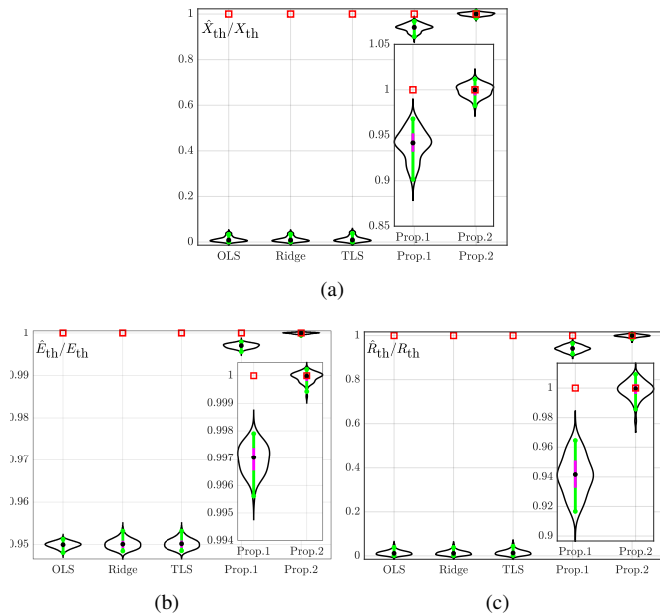


Fig. 9. Violin plots of TEP identification results under asynchronous measurements. The load type is a constant power load. $r_{PQ} = 0.2$. SNR is 20 dB. A Monte Carlo experiment is conducted with simulation parameters identical to those in Fig. 7.

The simulation results in Fig. 9 show that, despite the measurement delay, the proposed method maintains high identification accuracy, thanks to the sliding window technique. This approach effectively minimizes the impact of single-point errors, particularly for small time delays, where errors have a negligible effect. As a result, the data within the window can compensate for these errors, ensuring robust and accurate identification, and further validating the method's adaptability.

5) Effectiveness for High Data Collinearity

To further validate the effectiveness of the proposed method under conditions of high collinearity between active and reactive power, we set the correlation coefficients between P and Q to 0.95 and 0.99, to simulate the collinearity in real power grids. Monte Carlo experiments are conducted to obtain the TEP identification results of different methods under high collinearity, as shown in the violin plots in Fig. 10.

The simulation results in Fig. 10 show that, under high correlation between P and Q , the volatility of variance-based method proposed in this paper is slightly higher than that of mean-based method, but its unbiasedness is still well maintained. Both proposed methods significantly outperform the methods in the literature, especially under the extreme collinearity condition with a correlation coefficient of 0.99. In this case, the proposed methods effectively reduce estimation errors, demonstrating strong robustness.

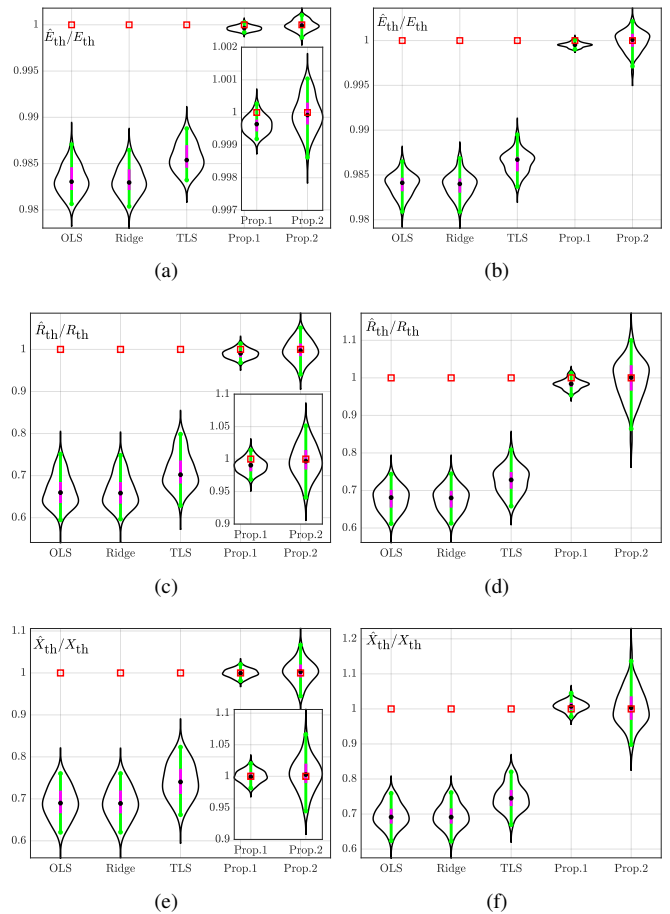


Fig. 10. Violin plots of TEP identification results under high data collinearity. (a), (c), (e) with $r_{PQ} = 0.95$. (b), (d), (f) with $r_{PQ} = 0.99$.

B. Practical Engineering Applications

In this section, the effectiveness of the proposed sensitivity and TEP identification method based on stochastic response statistical characteristics is demonstrated through case studies on the CloudPSS platform [30], [31].

Unlike the MATLAB platform, CloudPSS uses full electromagnetic transient (EMT) simulations, which calculate three-phase electrical quantities in real time and extract three-phase current and voltage magnitudes via a phase-locked loop (PLL) to compute power. This process involves multiple signal transformations and numerical computations, potentially introducing additional numerical and modeling errors. Furthermore, EMT simulations capture more complex electromagnetic phenomena and system dynamics, increasing error sources. EMT simulations provide a more accurate representation of the complexity and real behavior of power systems, making them more suitable for certain practical applications. This section, based on CloudPSS platform testing, further validates the effectiveness and robustness of the proposed method in different simulation environments.

The methods are tested using both principle model and the IEEE 39-bus system. The principle system is selected because obtaining the theoretical TEP values for large-scale systems through EMT simulations is difficult. Thus, the principle

model is used initially to evaluate the method's unbiasedness based on its theoretical TEP values.

1) Principle Model

To validate the proposed TEP identification methods, the principle model used in the simulation is shown in Fig. 1. The source voltage $E = 230$ kV. $X/R = 5$ based on typical ratios found in transmission and distribution systems, with impedance set as $R + jX = (10 + j50) \Omega$. The active and reactive powers of the random load are modeled using the bivariate correlated O-U random process as shown in Eq.31, with the same parameters as in Sec.IV-A and r_{PQ} of 0.2.

Fig. 11 presents a comparison of the performance of different methods (including literature methods and the proposed statistical characteristic-based method) in estimating the TEP. The violin plots provide a clear visual representation of the distribution differences in the TEP identification results.

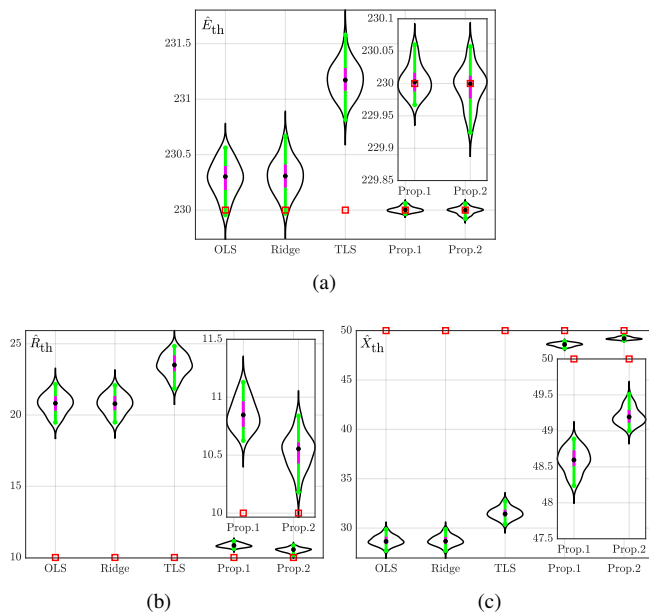


Fig. 11. Violin plots of TEP identification results of principle model in CloudPSS Platform. The simulation was performed with 50 independent Monte Carlo experiments, each simulating for 2 minutes. The sampling period $T_s = 0.005$ s and the sliding window size $W = 5$ s.

As shown in Fig. 11, the literature methods' TEP identification results display a wider probability distribution, with larger estimation biases and difficulty in accurately matching the theoretical values. These methods are more sensitive to system measurement noise. In contrast, the proposed methods show a significantly narrower distribution, with estimated values much closer to the theoretical ones. Particularly in the zoomed-in view, the high consistency between the estimated results and theoretical values is clearly evident. The distribution is more concentrated, significantly reducing both bias and variance, and demonstrating stronger robustness to noise. Overall, the proposed methods shows exceptional noise resistance and better meeting the requirements for online parameter identification in practical power systems.

2) IEEE 39-Bus System

This section uses the IEEE 39-bus system as the test system [33]. The full EMT model of the test system is developed on the CloudPSS platform.

For large-scale EMT systems, it's difficult to directly obtain the true values of TEP parameters. Identification based on step probing signals are typically used as reference values. Step probing signals can excite the steady-state response of the system, and their input-output relationship can be accurately estimated using methods like averaging, providing a reliable basis for identifying the system's static characteristics. This method is particularly suitable for scenarios where the input-output relationship is well-defined and can efficiently estimate the static sensitivity of the system.

In this study, a random step signal is superimposed on the active and reactive power of Bus 16 at the steady-state operating point to identify the true TEP values of Bus 16. The random step signal changes at a frequency of 1 Hz to a new random magnitude. The random magnitudes follow a normal distribution, and within each one-second interval, the signal magnitude remains constant until it changes to a new random value in the next second. The identified true TEP values for Bus 16 are $|E_{th}| = 500.77$ kV, $R_{th} = 7.06 \Omega$, and $X_{th} = 21.92 \Omega$.

The load at Bus 16 is set as a randomly fluctuating load, with the model given by Eq.31. r_{PQ} are set to 0.2 and 0.8, respectively. Through Monte Carlo simulations, the Violin plots of the TEP identification results for Bus 16 obtained using different methods are presented in Fig. 12.

Simulation results in Fig. 12 show that, with a low correlation coefficient, the TEP identification results from traditional methods exhibit a wide probability distribution range, with significant estimation bias, making it difficult to precisely match the theoretical values. These results are also more sensitive to system measurement noise. In contrast, with a high correlation coefficient, the identification results from traditional methods display even greater volatility, with a significant increase in numerical errors.

In comparison, even with a high correlation between P and reactive power Q , the proposed method maintains a more concentrated probability distribution, with estimation values closer to the theoretical values, significantly outperforming traditional methods. This demonstrates that using statistical characteristics based on the proposed sliding window method for TEP parameter identification can effectively reduce estimation errors and exhibit strong robustness.

V. CONCLUSION

This paper presents a novel method for identifying TEP based on the statistical characteristics of system's stochastic response. The method leverages stochastic fluctuation data under steady-state conditions, combined with sliding window techniques, to accurately calculate the sensitivity parameters between voltage magnitude–power and current magnitude–power, thereby achieving high precision and robustness in TEP identification. By analyzing statistical characteristics, such as mean, variance, and covariance, of the stochastic fluctuations within the sliding window, the method enables precise estimation of TEP.

Theoretical derivations and simulation results validate the robustness of the proposed method under challenging conditions, including low SNR, asynchronous measurements,

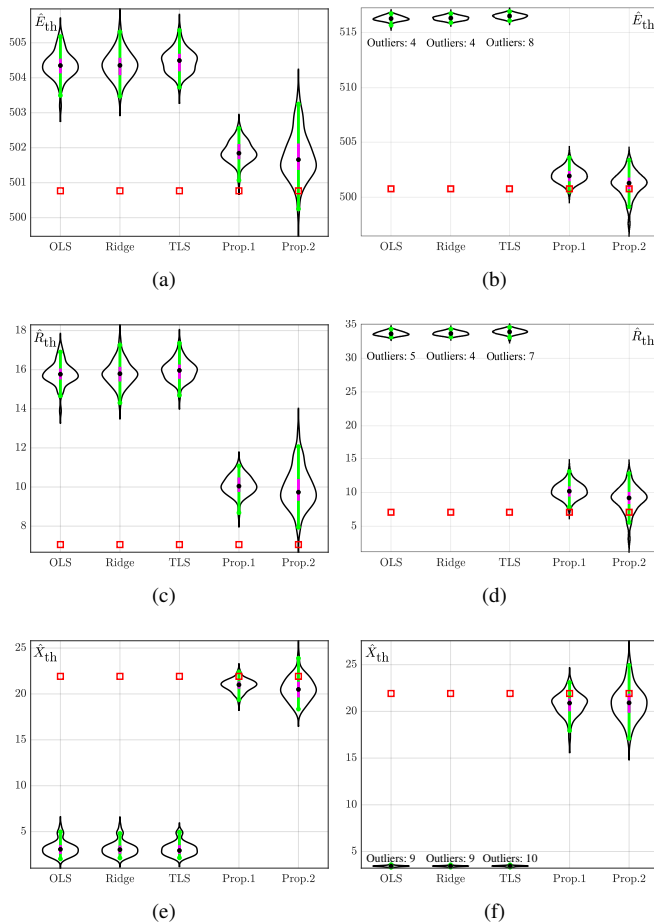


Fig. 12. Violin plots of TEP identification results in IEEE 39-bus system. (a), (c), (e) with $r_{PQ} = 0.2$. (b), (d), (f) with $r_{PQ} = 0.8$. The red box of the violin plots represents the reference values of the parameters. The sampling period $T_s = 0.005$ s and the sliding window size $W = 5$.

and data collinearity. Simulation results demonstrate that the method maintains strong adaptability and robustness, effectively addressing real-world issues encountered in power grids, and consistently achieving high identification accuracy despite these practical challenges.

REFERENCES

- [1] K. Vu, M. M. Begovic, D. Novosel, and M. M. Saha, "Use of local measurements to estimate voltage-stability margin," *IEEE Trans. Power Syst.*, vol. 14, no. 3, pp. 1029–1035, Aug. 1999.
- [2] F. Milano and R. Zárate-Miñano, "A systematic method to model power systems as stochastic differential algebraic equations," *IEEE Trans. Power Syst.*, vol. 28, no. 4, pp. 4537–4544, Nov. 2013.
- [3] G. Na, W. Song, C. Lu, and X. Chen, "Gaussian mixture models and its parameter estimation to describe the distributions of pmu random errors in power systems," in *2023 10th International Conference on Power and Energy Systems Engineering (CPSE)*, Nagoya, Japan, 2023, pp. 1–6.
- [4] S. Weckx, R. D'Hulst, and J. Driesen, "Voltage sensitivity analysis of a laboratory distribution grid with incomplete data," *IEEE Trans. Smart Grid*, vol. 6, no. 3, pp. 1271–1280, May 2015.
- [5] M. Kamel, F. Li, S. Bu, and Q. Wu, "A generalized voltage stability indicator based on the tangential angles of pv and load curves considering voltage dependent load models," *International Journal of Electrical Power & Energy Systems*, vol. 127, p. 106624, May 2021.
- [6] S. M. Abdelkader and D. J. Morrow, "Online thévenin equivalent determination considering system side changes and measurement errors," *IEEE Trans. Power Syst.*, vol. 30, no. 5, pp. 2716–2725, Sep. 2015.

- [7] S. M. Burchett *et al.*, "An optimal thévenin equivalent estimation method and its application to the voltage stability analysis of a wind hub," *IEEE Trans. Power Syst.*, vol. 33, no. 4, pp. 3644–3652, Jul. 2018.
- [8] M. M. Haji and W. Xu, "Online determination of external network models using synchronized phasor data," *IEEE Trans. Smart Grid*, vol. 9, no. 2, pp. 635–643, Mar. 2018.
- [9] H.-Y. Su and T.-Y. Liu, "Robust thévenin equivalent parameter estimation for voltage stability assessment," *IEEE Trans. Power Syst.*, vol. 33, no. 4, pp. 4637–4639, Jul. 2018.
- [10] N. Zhou, D. J. Trudnowski, J. W. Pierre, and W. A. Mittelstadt, "Electromechanical mode online estimation using regularized robust rls methods," *IEEE Trans. Power Syst.*, vol. 23, no. 4, pp. 1670–1680, Nov. 2008.
- [11] X. Wang, H. Sun, B. Zhang, W. Wu, and Q. Guo, "Real-time local voltage stability monitoring based on pmu and recursive least square method with variable forgetting factors," in *IEEE PES Innovative Smart Grid Technologies*, Tianjin, China, 2012, pp. 1–5.
- [12] G. Fusco, A. Losi, and M. Russo, "Constrained least squares methods for parameter tracking of power system steady-state equivalent circuits," *IEEE Trans. Power Del.*, vol. 15, no. 3, pp. 1073–1080, Jul. 2000.
- [13] A. Malkhandi, N. Senroy, and S. Mishra, "A dynamic model of impedance for online thevenin's equivalent estimation," *IEEE Trans. Circuits Syst. II: Exp. Briefs*, vol. 69, no. 1, pp. 194–198, Jan. 2022.
- [14] S. Corsi and G. Taranto, "A real-time voltage instability identification algorithm based on local phasor measurements," *IEEE Trans. Power Syst.*, vol. 23, no. 3, pp. 1271–1279, Aug. 2008.
- [15] C. Wang, Z. Qin, Y. Hou, and J. Yan, "Multi-area dynamic state estimation with pmu measurements by an equality constrained extended kalman filter," *IEEE Trans. Smart Grid*, vol. 9, no. 2, pp. 900–910, Mar. 2018.
- [16] E. Peker and A. Wiesel, "Fitting generalized multivariate huber loss functions," *IEEE Signal Process. Lett.*, vol. 23, no. 11, pp. 1647–1651, Nov. 2016.
- [17] B. Alinezhad and H. K. Karegar, "On-line thévenin impedance estimation based on pmu data and phase drift correction," *IEEE Trans. Smart Grid*, vol. 9, no. 2, pp. 1033–1042, Mar. 2018.
- [18] A. R. R. Matavalam and V. Ajarapu, "Sensitivity based thevenin index with systematic inclusion of reactive power limits," *IEEE Trans. Power Syst.*, vol. 33, no. 1, pp. 932–942, Jan. 2018.
- [19] I. Smon, G. Verbic, and F. Gubina, "Local voltage-stability index using tellgen's theorem," *IEEE Trans. Power Syst.*, vol. 21, no. 3, pp. 1267–1275, Aug. 2006.
- [20] X. Zhang, D. Shi, X. Lu, Z. Yi, Q. Zhang, and Z. Wang, "Sensitivity based thevenin index for voltage stability assessment considering n-1 contingency," in *2018 IEEE Power & Energy Society General Meeting (PESGM)*, Portland, OR, USA, 2018, pp. 1–5.
- [21] J. Zhang, X. Zheng, Z. Wang, L. Guan, and C. Y. Chung, "Power system sensitivity identification—Inherent system properties and data quality," *IEEE Trans. Power Syst.*, vol. 32, no. 4, pp. 2756–2766, Jul. 2017.
- [22] Y. C. Chen, J. Wang, A. D. Domínguez-García, and P. W. Sauer, "Measurement-based estimation of the power flow jacobian matrix," *IEEE Trans. Smart Grid*, vol. 7, no. 5, pp. 2507–2515, Sep. 2016.
- [23] E. L. d. Silva *et al.*, "Data-driven sensitivity coefficients estimation for cooperative control of pv inverters," *IEEE Trans. Power Del.*, vol. 35, no. 1, pp. 278–287, Feb. 2020.
- [24] Z. Tang, Y. Liu, T. Liu, X. Xu, and J. Liu, "Adaptive weighted ridge regression estimator for time-varying sensitivity identification," *IEEE Trans. Power Syst.*, vol. 39, no. 1, pp. 2377–2380, Jan. 2024.
- [25] Y. Liang, J. Zhao, P. Siano, and D. Srinivasan, "Temporally-adaptive robust data-driven sparse voltage sensitivity estimation for large-scale realistic distribution systems with pvs," *IEEE Trans. Power Syst.*, vol. 38, no. 4, pp. 3977–3980, Jul. 2023.
- [26] J.-W. Chang, M. Kang, and S. Oh, "Data-driven estimation of voltage-to-power sensitivities considering their mutual dependency in medium voltage distribution networks," *IEEE Trans. Power Syst.*, vol. 37, no. 4, pp. 3173–3176, Jul. 2022.
- [27] S. Talkington, D. Turizo, S. Grijalva, J. Fernandez, and D. K. Molzahn, "Conditions for estimation of sensitivities of voltage magnitudes to complex power injections," *IEEE Trans. Power Syst.*, vol. 39, no. 1, pp. 478–491, Jan. 2024.
- [28] M. Adeen and F. Milano, "Modeling of correlated stochastic processes for the transient stability analysis of power systems," *IEEE Trans. Power Syst.*, vol. 36, no. 5, pp. 4445–4456, Sep. 2021.
- [29] G. Akemann, J. Baik, and P. D. Francesco, *The Oxford Handbook of Random Matrix Theory*. Oxford University Press, 2011.

- [30] Y. Song, Y. Chen, Z. Yu, S. Huang, and C. Shen, "Cloudpss: A high-performance power system simulator based on cloud computing," *Energy Reports*, vol. 6, pp. 1611–1618, 2020.
- [31] "Ms windows nt kernel description," 2017, accessed: Jun. 24, 2022. [Online]. Available: <https://www.cloudpss.net/>
- [32] F. Bizzarri, D. d. Giudice, S. Grillo, D. Linaro, A. Brambilla, and F. Milano, "Inertia estimation through covariance matrix," *IEEE Trans. Power Syst.*, vol. 39, no. 1, pp. 947–956, Jan. 2024.
- [33] T. Athay, R. Podmore, and S. Virmani, "A practical method for the direct analysis of transient stability," *IEEE Trans. Power App. Syst.*, vol. PAS-98, no. 2, pp. 573–584, Mar. 1979.

APPENDIX A

The complete formula for identifying TEP based on magnitude sensitivity is

$$\left\{ \begin{array}{l} \beta_{|V|P} = -\frac{(R_{th}^2 + X_{th}^2)\tilde{P}_k + R_{th}|\tilde{V}_k|^2}{|\tilde{V}_k|\sqrt{\tilde{\Delta}}} \\ \beta_{|V|Q} = -\frac{(R_{th}^2 + X_{th}^2)\tilde{Q}_k + X_{th}|\tilde{V}_k|^2}{|\tilde{V}_k|\sqrt{\tilde{\Delta}}} \\ \beta_{|I|P} = \frac{\tilde{P}_k + R_{th}|\tilde{I}_k|^2}{|\tilde{I}_k|\sqrt{\tilde{\Delta}}} \\ \beta_{|I|Q} = \frac{\tilde{Q}_k + X_{th}|\tilde{I}_k|^2}{|\tilde{I}_k|\sqrt{\tilde{\Delta}}} \\ |\tilde{V}_k| = \sqrt{\frac{|E_{th}|^2 - 2(R_{th}\tilde{P}_k + X_{th}\tilde{Q}_k) + \sqrt{\tilde{\Delta}}}{2}} \\ |\tilde{I}_k| = \sqrt{\frac{|E_{th}|^2 - 2(\tilde{P}_k R_{th} + \tilde{Q}_k X_{th}) - \sqrt{\tilde{\Delta}}}{2(R_{th}^2 + X_{th}^2)}} \end{array} \right. \quad (35)$$

with discriminant $\tilde{\Delta} = E_{th}^4 - 4(R_{th}\tilde{P}_x + X_{th}\tilde{Q}_x)E_{th}^2 - 4(X_{th}\tilde{P}_x - R_{th}\tilde{Q}_x)^2$.